

## Pharmacophore Guided Discovery of Small-Molecule Human Apurinic/Apyrimidinic Endonuclease 1 Inhibitors

Zahrah Zawahir, Raveendra Dayam,<sup>§</sup> Jinxia Deng, Cherelene Pereira, and Nouri Neamati\*

Department of Pharmacology and Pharmaceutical Sciences, School of Pharmacy, University of Southern California, 1985 Zonal Avenue, Los Angeles, California 90033

Received June 17, 2008

Human apurinic/aprimidinic endonuclease 1 (APE1) is an important enzyme in the base excision repair (BER) pathway that is essential for the repair of abasic sites in the genome. Evidence for APE1 as an attractive therapeutic target in anticancer drug development has been demonstrated by studies that link overexpression of APE1 in many cancers to resistance of tumor cells to radio- and chemotherapy. APE1 also shows a protective effect in several cancer cell models to a variety of DNA damaging agents. This study represents the first rational design of selective small-molecule APE1 inhibitors utilizing a three-dimensional interaction-based pharmacophore perception. All of our most potent molecules show inhibitory activity below 10  $\mu$ M and are selective for APE1 inhibition.

### Introduction

In mammalian cells, reactive oxygen species, alkylation, deamination, and other processes of cellular metabolism and/or exogenous drug toxicity can cause endogenous mutagenic and cytotoxic DNA base lesions that are predominantly repaired by the base excision repair (BER<sup>q</sup>) pathway. BER is initiated by lesion-specific glycosylases that excise the damaged base from the sugar–phosphate backbone, resulting in a potentially cytotoxic apurinic/aprimidinic (AP) site intermediate that becomes the substrate for the major human AP endonuclease (APE1, also known as Ref-1).<sup>1</sup> APE1 is a fundamental protein in this essential repair pathway and is thought to be responsible for >95% of total AP endonuclease activity in human cell culture extracts.<sup>1,2</sup> The enzyme belongs to the highly conserved ExoIII/Xth family of endonucleases, of which the prototypical *Escherichia coli* homologue exonuclease III is a member. A second family of AP endonucleases, EndoIV, contains the *E. coli* endonuclease IV, for which no human counterpart appears to exist. The other mammalian enzyme responsible for AP site repair is APE2, which belongs to the APE2/APN family of enzymes, a subclass of the ExoIII/Xth family, bearing greatest similarity to the *Saccharomyces cerevisiae* APN2 gene product.<sup>3–5</sup>

Following excision of the damaged base, APE1 hydrolytically cleaves the phosphodiester backbone 5' to the AP site, leaving a 3'-hydroxyl and a 5' abasic deoxyribose phosphate to be processed by the subsequent cascade of BER enzymes, including DNA polymerase beta and DNA ligase III.<sup>6,7</sup> APE1 activity is requisite for rectification of DNA damage in both the short-patch and long-patch subpathways of BER, although each pathway utilizes different enzymes to complete repair subsequent to APE1 activity. In addition to its primary AP site incision function, APE1 also exhibits 3'  $\rightarrow$  5' exonuclease, 3'-phos-

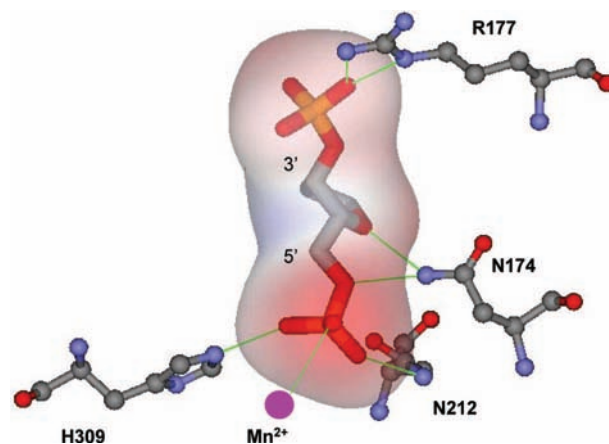


**Figure 1.** APE1 interactions with abasic site fragment in the cocrystal structures of human APE1 bound AP DNA (PDB: 1DEW and 1DE9). The abasic site fragment is rendered as a stick model. The surface model of the abasic site fragment colored according to electrostatic potentials is also shown. APE1 active site amino acid residues are shown as ball and stick models. The green lines indicate interactions and magenta sphere represents the active site  $\text{Mn}^{2+}$ . Some of the interactions are considered in three-dimensional pharmacophore modeling.

phodiesterase, and RNase H catalysis, and a 3'-phosphatase activity.<sup>8,9</sup> It has also been shown that APE1 appears to have endonucleolytic activity as a repair enzyme within the nucleotide incision repair pathway.<sup>10</sup> The same catalytic active site, found in the conserved domain of most members of the ExoIII family, appears to be employed for all of these repair actions.<sup>11</sup> The active site region also shares some similarity with  $\text{Mg}^{2+}$ -dependent endonucleases, phosphatases, and proteins involved in cell cycle signaling and transduction.<sup>12</sup> In addition to its repertoire of repair activity, and equally as essential in function, APE1 utilizes a site located in its N-terminus for redox regulation of important transcription factors such as NF- $\kappa$ B, p53, c-Fos, and c-Jun.<sup>13,14</sup> This redox function of the enzyme was discovered simultaneously to its endonuclease function, hence an alternate name of Ref-1.<sup>15</sup> Our investigation focuses on the inhibition of APE1 endonuclease activity.

Given the results of studies that have used RNA interference methods to suppress APE1 expression, this essential enzyme

\* To whom correspondence should be addressed. Phone: (323) 442 2341. Fax: (323) 442 1681. E-mail: neamati@usc.edu.

<sup>§</sup> Current Address: Informatics Division, GVK Biosciences Private Limited, Hyderabad, India.

<sup>q</sup> Abbreviations: BER, base excision repair; APE1, human apurinic/aprimidinic endonuclease 1; ref-1, redox effector factor-1; ExoIII, exonuclease III; EndoIV, endonuclease IV; APE2, human apurinic/aprimidinic endonuclease 2; APN, yeast apurinic/aprimidinic endonuclease; HIV-1, human immunodeficiency virus 1; GOLD, genetic optimization for ligand docking; eHITS, electronic high-throughput screening.

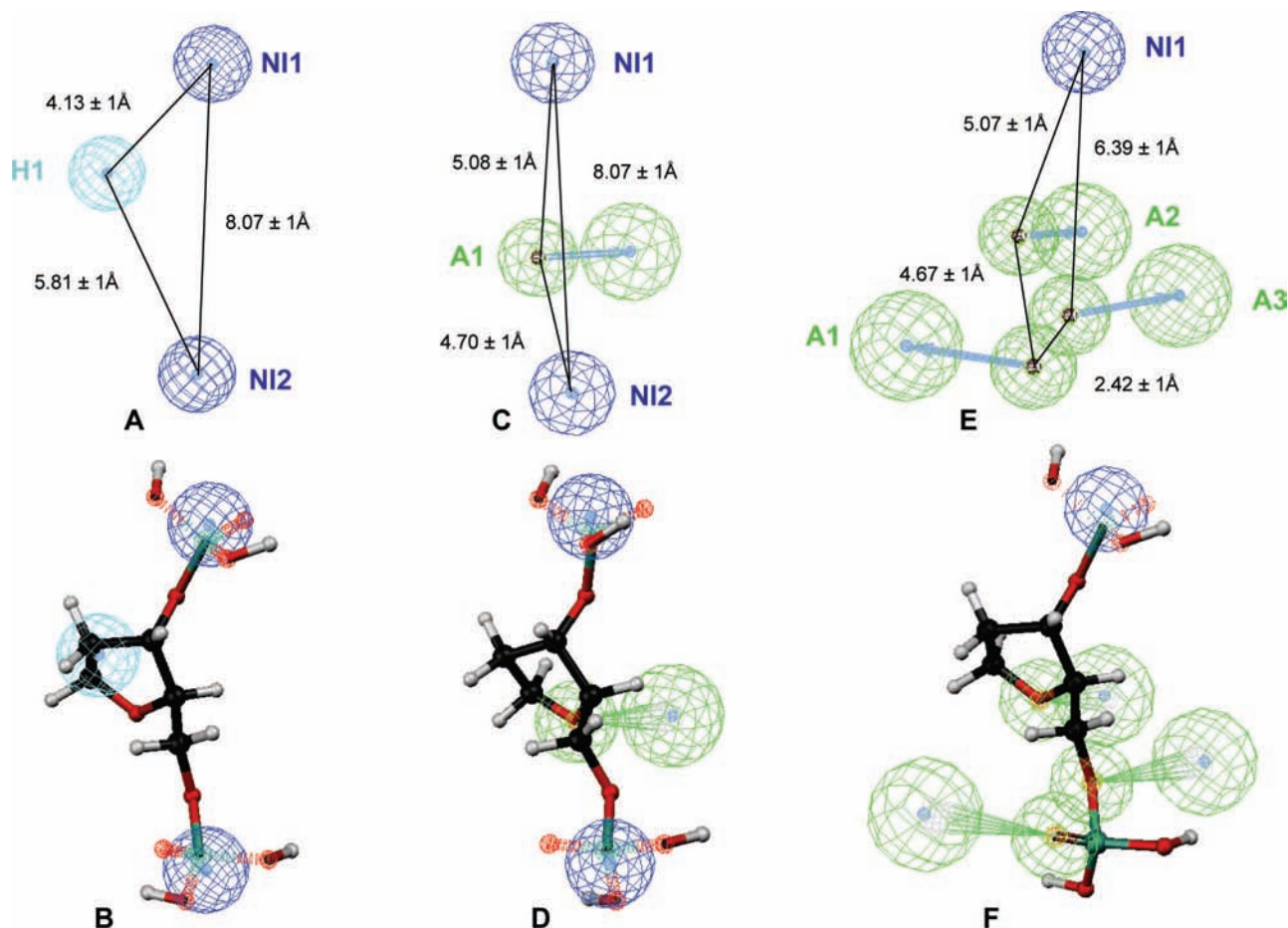


**Figure 2.** Three-dimensional pharmacophore models H1NI2 (A), A1NI2 (C), and A3NI1 (E) are generated to represent human APE1 interactions with abasic DNA in the cocrystal structure of the APE1 bound to abasic DNA (PDB: 1DEW). The abasic fragment (3'-phosphate, abasic deoxyribose, and 5'-phosphate) was used as a template for pharmacophore modeling. Pharmacophore features are: Hydrophobic (H, cyan), negatively ionizable (NI, blue), H-bond acceptor (A, green). Interfeatures distances are given in Å. (B,D,F) The pharmacophore models are mapped on to the abasic fragment.

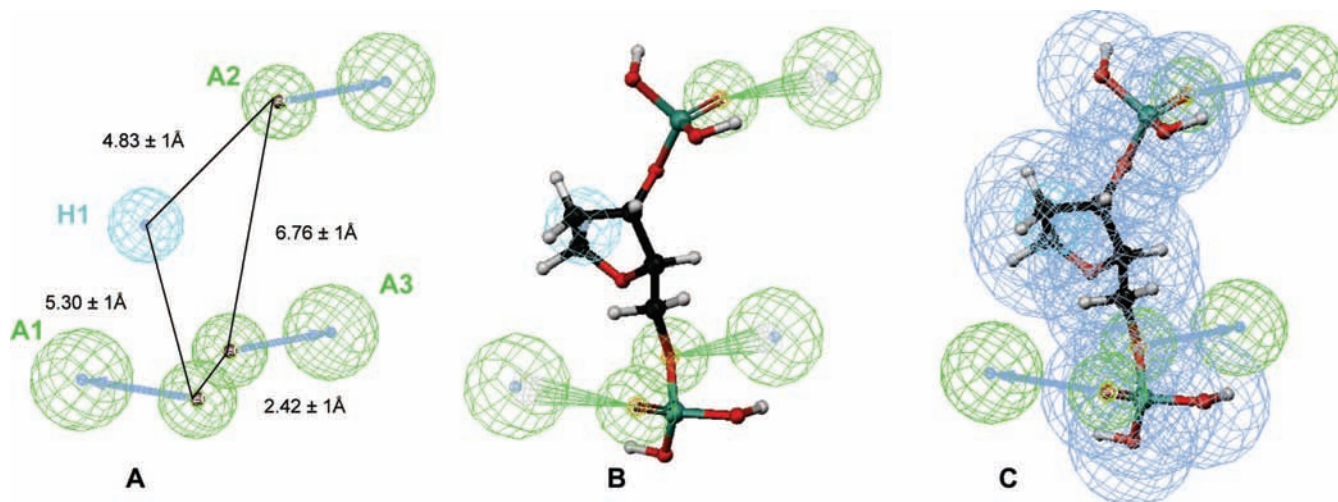


**Figure 3.** (A) Three-dimensional pharmacophore model (A3H1) was based on the human APE1 interactions with abasic DNA in the cocrystal structure of human APE1 bound to abasic DNA (PDB: 1DEW). The abasic fragment was used as a template for pharmacophore modeling. (B) The pharmacophore model was mapped on to the abasic fragment. (C) The shape of the abasic fragment was generated and merged with the H1A3 pharmacophore. Pharmacophore features are: Hydrophobic (H, cyan), negatively ionizable (NI, blue), H-bond acceptor (A, green). The light-blue mesh shows shape of the abasic fragment.

presents itself as an attractive target in anticancer drug development. The intracellular consequences of antisense targeted APE1 depletion include sensitization of many cancer cell types to a variety of cytotoxic alkylating agents, oxidizing agents, and

ionizing radiation.<sup>16–18</sup> Furthermore, a recent study shows that in colon cancer cells, strong APE1 downregulation causes cell proliferation to be retarded and unrepaired abasic damage accumulates to levels sufficient to provoke apoptosis.<sup>19</sup> Blocking

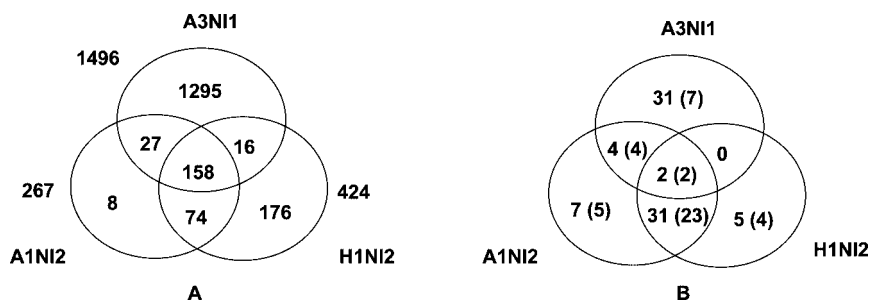


**Figure 4.** (A) Venn diagram shows the number of compounds retrieved by pharmacophore models A3NI1, H1NI2, and A1NI2 from a database of 362360 compounds. The compounds in intersection area are common hits for respective pharmacophore models. (B) Venn diagram shows number of compounds tested in an in vitro assay specific to APE1. Compounds in parenthesis inhibited APE1 with an  $IC_{50}$  value  $< 100 \mu M$ .

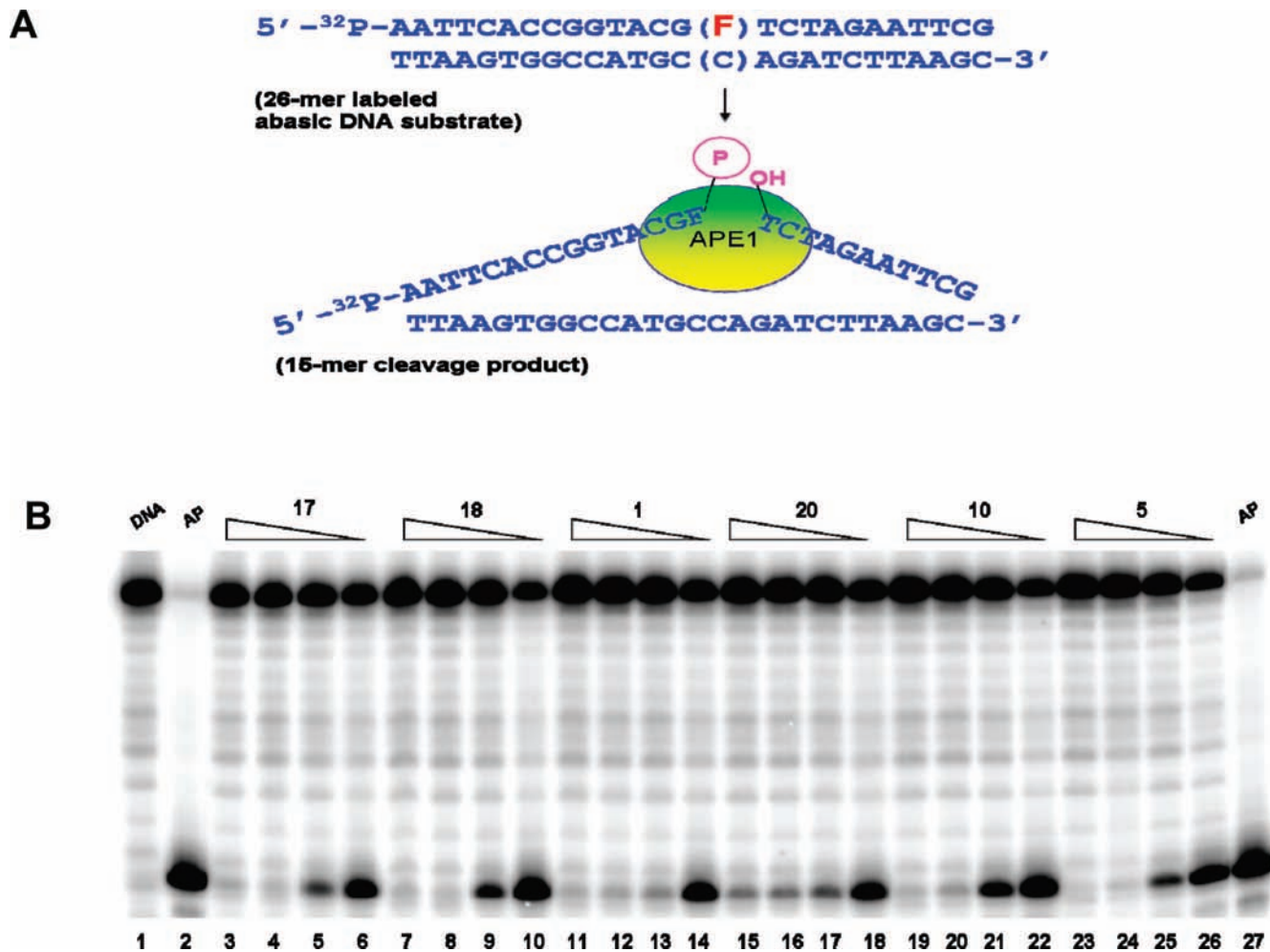


**Figure 5.** (A) A 25-mer oligonucleotide 5'-labeled with  $P^{32}$  and containing an abasic site analog, tetrahydrofuran (F), is used in an assay to determine relative abasic site incision activity of recombinant purified human APE1. (B) A representative SDS-PAGE of the most active APE1 inhibitory molecules in the assay. Lane 1: DNA only, lanes 2 and 27: APE1 + DMSO only, lanes 3–6: compound 17; lanes 7–10: compound 18; lanes 11–14: compound 1; lanes 15–18: compound 20; lanes 19–22: compound 10; lanes 23–26: compound 5. All compounds were tested at 100, 33, 11, and 3.7  $\mu M$ .

APE1 repair activity with methoxyamine, a small molecule that binds irreversibly to abasic sites sensitizes ovarian and colon cell lines to treatment with Temozolomide, as does using a dominant-negative form of APE1 in lung cancer cells.<sup>20</sup>

In addition to demonstrable potentiation of the effects of cytotoxic agents, the value of concurrent APE1 inhibition with existing anticancer clinical regimens is underscored by clinical evidence that establishes a relationship between APE1 expression levels and cancer. Alterations in APE1 expression and localization are thought to have prognostic and/or predictive significance in several cancers, including colon, breast, and

lung.<sup>21–23</sup> Differential patterns of expression between normal and cancerous tissue have been observed in cervical, prostate, and epithelial ovarian cancers, where expression levels are elevated.<sup>24–27</sup> A predictive significance in cancer-specific survival following radiotherapy has also been attributed to APE1 expression.<sup>28,29</sup>

Recently, there has been a significant effort toward identifying inhibitors to mammalian DNA repair proteins in keeping with the emerging concept in anticancer drug development that sensitizing cancer tissue to core chemotherapeutic regimens by simultaneously hindering DNA repair may result in enhanced



**Table 1.** APE1 Inhibitory Activity of Compounds Retrieved Using Pharmacophore Models H1NI2, A1NI2, A3NI1

S.No.	Structure	Activity IC <sub>50</sub> (μM)	S.No.	Structure	Activity IC <sub>50</sub> (μM)
<b>1</b> H1NI2		4 ± 1	<b>12</b> H1-A1-NI2		8 ± 2
<b>2</b> H1NI2		9 ± 1	<b>13</b> H1-A1-NI2		11 ± 2
<b>3</b> A1NI2		17 ± 3	<b>14</b> H1-A1-NI2		20
<b>4</b> H1-A1-NI2		15 ± 6	<b>15</b> H1-A1-NI2		19 ± 9
<b>5</b> H1-A1-NI2		4 ± 1	<b>16</b> H1-A1-NI2		26 ± 6
<b>6</b> H1-A1-NI2		15	<b>17</b> A1NI2-A3NI1		6 ± 1
<b>7</b> H1-A1-NI2		16 ± 4	<b>18</b> A1NI2-A3NI1		6 ± 1
<b>8</b> H1-A1-NI2		22	<b>19</b> A1NI2-A3NI1		8 ± 1
<b>9</b> H1-A1-NI2		20	<b>20</b> A1NI2-A3NI1		4 ± 1
<b>10</b> H1-A1-NI2		6 ± 3	<b>21</b> A3NI1		20 ± 2
<b>11</b> H1-A1-NI2		12 ± 2			

therapeutic outcomes.<sup>30</sup> A compound with inhibitory activity against APE1 *in vitro* has been demonstrated to potentiate the cytotoxicity of a variety of selective DNA-damaging agents in a human fibrosarcoma cell line.<sup>31</sup> In addition, antimony-containing small-molecule inhibitors of APE1 have been reported that show high cytotoxicity.<sup>32</sup>

Rational design of small-molecule APE1 inhibitors is enabled by the availability of structural information on APE1 in complex with the substrate DNA bearing an abasic site. The pharmacophore perception of identifying small-molecule inhibitors with diverse chemical scaffolds is a popular technique in drug design and has been successfully used to discover numerous classes of clinically relevant small-molecule inhibitors targeting a number of pathways, including DNA repair.<sup>33–35</sup> We have developed a set of three-dimensional (3D) pharmacophore models based on APE1 interactions with the abasic deoxyribose

3'- and 5'-phosphate backbone in a co-crystal structure of APE1 in complex with substrate abasic DNA.<sup>36</sup> The pharmacophore models represent prominent interactions and the chemical nature and shape of the abasic DNA fragment within the APE1 active site. This is the first report of rationally designed selective APE1 inhibitors.

In an effort to characterize the selectivity and mode of inhibition of these compounds against APE1, we further evaluated them against the catalytic activity of Exonuclease III (ExoIII), Endonuclease IV (EndoIV), and HIV-1 integrase. While both ExoIII and EndoIV are enzymes that possess abasic site cleavage activity, HIV-1 integrase is a retroviral enzyme that binds to the viral and host DNA and, similar to APE1, cleaves the phosphodiester backbone 5' to its recognition site of the viral DNA, leaving a recessed 3'hydroxyl moiety. As with APE1 and ExoIII, and characteristic of most DNA-binding

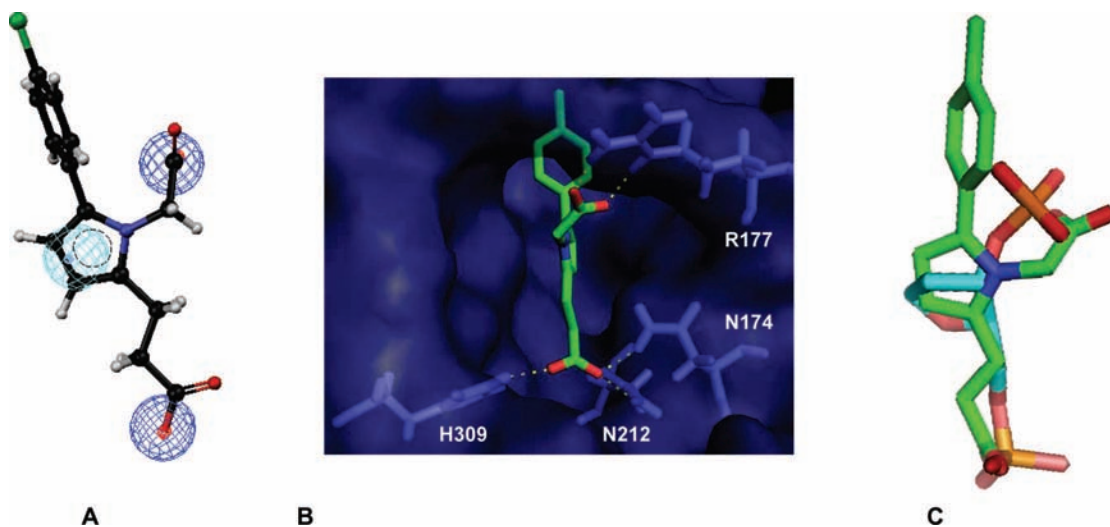


**Figure 6.** (A) Compound **1** mapped onto pharmacophore H1NI2. There is a good agreement between chemical features of compound **1** and pharmacophoric features of H1NI2. (B) The predicted bound conformation of compound **1** inside the abasic DNA binding site of APE1. The blue surface represents abasic DNA binding region of APE1. Compound **1** is shown as a stick (green) model. Compound **1** interactions with prominent amino acid residues of APE1 are shown as dashed-lines. There is a strong agreement between mapped pharmacophoric features of compound **1** and its interactions with prominent amino acid residues of APE1 active site. (C) The predicted bound conformation of compound **1** is superimposed onto the bound orientation of abasic unit in the cocrystal structure of APE1-abasic DNA complex (PDB: 1DEW).

**Table 2.** APE1 Inhibitory Activity of Analogues of Compounds **1** and **2**

S.No.	Structure	Activity IC <sub>50</sub> (μM)
<b>1</b> H1NI2		4 ± 1
<b>2</b> H1NI2		9 ± 1
<b>22</b>		12 ± 3
<b>23</b>		9 ± 1

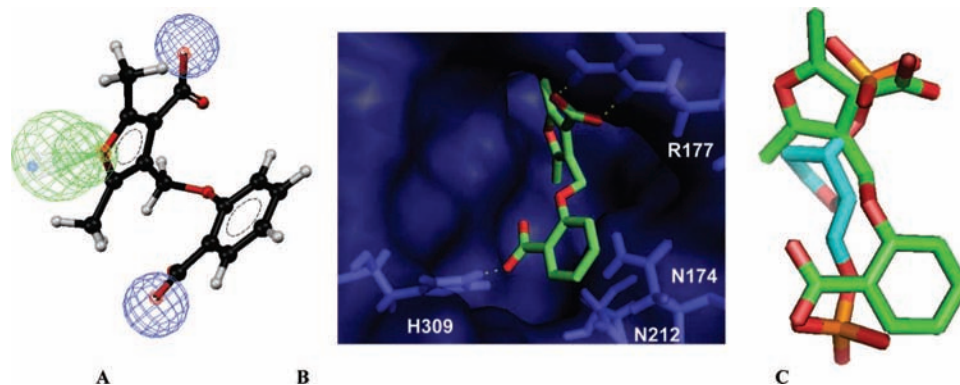
enzymes, HIV-1 integrase also requires a divalent metal cation for catalysis. Importantly, this structurally diverse set of molecules we have identified are selective APE1 inhibitors and are suitable as lead molecules to establish quantitative structure–activity relationship models for further development of clinically relevant APE1 inhibitors.

## Results and Discussion

**Design and Generation of Pharmacophore Models.** APE1 uses a well-defined positively charged surface to selectively recognize the flipped-out abasic DNA fragment, which binds within a unique binding pocket on the bottom of the DNA binding region of APE1.<sup>36</sup> Charge interactions, several strong H-bonding interactions, and shape complementarity are observed between prominent amino acid residues of APE1 and abasic fragment of the abasic DNA (Figure 1). An unusual interaction between the APE1 amino acid residue Arg177, which inserts

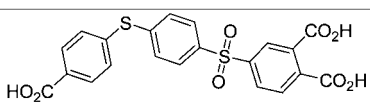
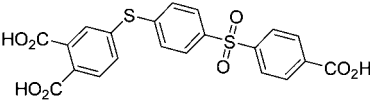
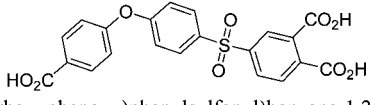
through the major groove of abasic DNA and the negatively charged 3'-phosphate of the abasic fragment indicate unique functionality for this enzyme. A hydrophobic pocket surrounded by amino acid residues Phe253, Trp280, and Ile282, selectively recognizes and binds to the abasic deoxyribose sugar moiety and prohibits binding of DNA bases and racemized β-anomer abasic sites. The negatively charged 5'-phosphate is involved in a number of strong charge and H-bonding interactions with APE1 amino acid residues Asn174, Asn212, His309, and the Mn<sup>2+</sup> metal ion (Figure 1).

Given the importance and uniqueness of these interactions for APE1 in recognizing and incising abasic DNA sites, we transformed the prominent ones into a set of 3D pharmacophore models using the abasic fragment as a template. These pharmacophore models represent the chemical and electrostatic environment of specific APE1 interactions with the abasic DNA fragment (Figures 2–3). The co-crystal structures used to



**Figure 7.** (A) Compound **17** mapped onto pharmacophore A1NI2. (B) The predicted bound conformation of compound **17** inside the abasic DNA binding site of APE1. The blue surface represents abasic DNA binding region of APE1. Compound **17** is shown as a green stick model. Compound **17** interactions with prominent amino acid residues (stick models) of APE1 are shown as yellow dashed lines. (C) The predicted bound conformation of compound **17** is superimposed onto the bound orientation of the abasic unit in the cocrystal structure of APE1-abasic DNA complex (PDB: 1DEW).

**Table 3.** APE1 Inhibitory Activity of Analogues of Compound **5**

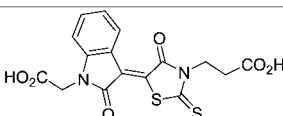
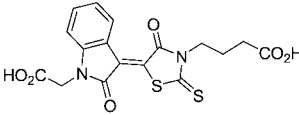
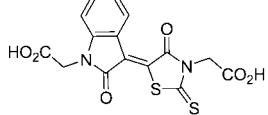
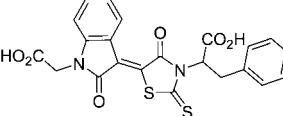
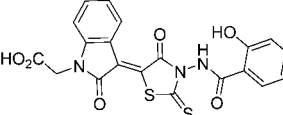
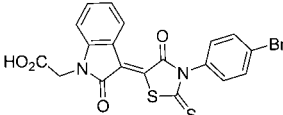
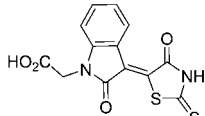
S.No.	Structure	Activity IC <sub>50</sub> (μM)
<b>5</b> H1-A1- NI2	 4-(4-(4-carboxyphenylthio)phenylsulfonyl)benzene-1,2-dioic acid	4 ± 1
<b>24</b>	 4-((4-(4-carboxyphenylsulfonyl)phenyl)sulfanyl)benzene-1,2-dioic acid	6 ± 2
<b>25</b>	 4-(4-(4-carboxyphenoxy)phenylsulfonyl)benzene-1,2-dioic acid	10

generate the pharmacophore models contains a synthetic analog (tetrahydrofuran) of the abasic deoxyribose. The natural hydrolytic abasic deoxyribose site harbors a hydroxyl group. Interactions of the protein with the abasic fragment are represented by a set of pharmacophore components: hydrophobic (H), H-bond acceptor (A), and negatively ionizable (NI) features. The pharmacophore models were then used to identify novel molecules bearing desired chemical moieties that mimic abasic DNA to bind APE1 and disrupt its catalytic functions.

Four plausible pharmacophore models were generated using a combination of H, A, and NI features (Figures 2–3). The pharmacophore H1NI2 is comprised of two negatively ionizable (NI1–NI2) and a hydrophobic (H1) feature (Figure 2A). The NI1 and NI2 features are separated by  $8.07 \pm 1$  Å. The interfeature distances between H1 to NI1 and NI2 are  $4.13 \pm 1$  and  $5.81 \pm 1$  Å, respectively. Mapping the H1NI2 pharmacophore onto the abasic fragment demonstrates that the NI1 and NI2 features represent the negatively charged 3'- and 5'-phosphates and the H1 feature corresponds to the tetrahydrofuran that mimics the natural abasic deoxyribose (Figure 2B). Pharmacophore A1NI2 consists of one A feature and two NI (NI1 and NI2) features. Similar to pharmacophore H1NI2, the NI1 and NI2 features are separated by a distance of  $8.07 \pm 1$  Å. The mapping of A1NI2 onto the abasic fragment shows a feature mapping pattern similar to that of pharmacophore H1NI2 with respect to the NI1 and NI2 features. The H-bond acceptor feature

is mapped onto the O atom of the tetrahydrofuran (Figure 2C–D). Interfeature distances between A1 to NI1 and NI2 are  $5.08 \pm 1$  and  $4.70 \pm 1$  Å, respectively. The pharmacophore A3NI1 is comprised of three H-bond acceptor (A1–A3) features and a negatively ionizable feature (NI1). The NI1 feature represents the negatively charged 3'-phosphate of the abasic fragment. One of the three H-bonding acceptor features (A1) represents the interaction of the tetrahydrofuran oxygen atom with the side chain amine of Asn174. H-bonding acceptor features A2–A3 represent interactions of APE1 amino acid residues Asn174, His309 with the O5', and O1P oxygen atoms of the 5'-phosphate. The 3D arrangement of features and mapping of pharmacophore A3NI1 onto the abasic fragment is shown in Figures 2E–F. In parallel to the above-mentioned three pharmacophore models, the model A3H1 was also generated, which is devoid of a negatively ionizable feature. The pharmacophore A3H1 consists of three H-bond acceptor features (A1–A3) and a hydrophobic feature (H1). The 3D arrangement and interfeature distances of A3H1 are shown in Figure 3A. Mapping the A3H1 pharmacophore onto the abasic fragment correlates the APE1-abasic DNA fragment interactions (Figure 3B). The H-bond acceptor feature A1 represents the 3'-phosphate interaction with the side chain guanidine of Arg177. The hydrophobic feature H1 demonstrates the chemical nature and environment of the tetrahydrofuran that mimics the natural abasic deoxyribose. The cocrystal structures used to generate

**Table 4.** APE1 Inhibitory Activity of Analogues of Compounds **10** and **11**

S.No.	Structure	Activity IC <sub>50</sub> (μM)
<b>10</b> H1-A1- NI2		6 ± 3
<b>11</b>		12 ± 2
<b>26</b>		13 ± 6
<b>27</b>		3 ± 1
<b>28</b>		11 ± 2
<b>29</b>		6 ± 3
<b>30</b>		9 ± 3

2-((Z)-2-oxo-3-(4-oxo-2-thioxothiazolidin-5-ylidene)indolin-1-yl)acetic acid

the pharmacophore used the synthetic analogue to the natural hydrolytic abasic site, which harbors a hydroxyl group. The H-bond acceptor features A2–A3 correlate to the interactions of residues Asn174, His309 with the O5', and O1P oxygen atoms of the 5'-phosphate. In addition to considering interaction features, the shape of the abasic fragment backbone was also generated and merged with pharmacophore A3H1 to enhance its selectivity (Figure 3C). The shape feature functions as an additional filter in the database search process and restricts the shape and size of hits that can be retrieved by pharmacophore A3H1.

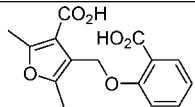
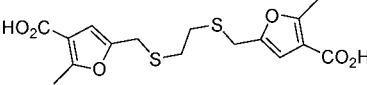
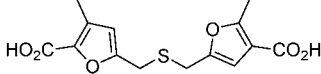
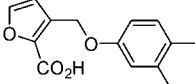
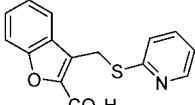
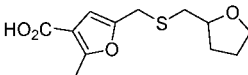
**Database Search and Compound Selection.** A library of 365000 commercially available small-molecule compounds was collected and converted to a searchable multiconformer 3D database. The small-molecule database was searched for potential compounds using the 3D pharmacophore models H1NI2, A1NI2, A3NI, and A3H1 as search queries. A search using pharmacophore H1NI2 retrieved 424 compounds (0.0011%). The database search using pharmacophore models A1NI2 and A3NI1 retrieved 267 (0.0007%) and 1496 (0.0041%) compounds, respectively. The pharmacophore A3H1 retrieved a large number of hits, approximately 10% of the database. The high hit rate corresponds to the nonselective nature of the pharmacophore. In addition, the short interfeature distances of various features in A3H1 contributed to the high hit rate (Figure 3A). On the contrary, pharmacophore S1A3H1, which incorporated the shape of the nucleotide backbone, retrieved 1830 compounds (0.005%). Pharmacophore models H1NI2, A1NI2,

and A3NI1 possessed considerable similarity in nature and arrangement of pharmacophore features. Pharmacophore models H1NI2 and A1NI2 have two NI features in a similar 3D arrangement. Pharmacophore models A1NI2 and A3NI1 have a NI and an A feature in common, while H1NI2 and A3NI1 have a NI feature in common. The observed similarity among H1NI2, A1NI2, and A3NI1 prompted us to look for compounds common for these three pharmacophore models. Interestingly, a significant number of compounds were found to be included in all models that share at least a negatively ionizable feature (Figure 4A). There were 158 compounds found in common for pharmacophore models H1NI2, A1NI2, and A3NI1. There were 74 compounds found in common for H1NI2 and A1NI2. Pharmacophore A3NI1 retrieved 27 and 16 compounds common to A1NI2 and H1NI2, respectively. Of the 1754 total hits retrieved by pharmacophore models H1NI2, A1NI2, and A3NI1, 80 compounds were selected from common and individual pharmacophore hits for an in vitro screening assay against APE1 (Figure 4B). Additionally, 80 compounds were selected from 1830 hits retrieved by the shape merged pharmacophore S1A3H1. Compounds were selected based on pharmacophore fit value, pharmacophore mapping pattern, predicted binding orientation, and interactions of the compounds within the active site of APE1. Docking conformations for all of the molecules discussed were performed using GOLD.<sup>37</sup>

**Selective Inhibition of APE1 Catalytic Activity by Structurally Diverse Small Molecules.** Two sets of structurally diverse compounds were selected to screen in an in vitro assay specific to APE1. These molecules were tested in an electrophoretic APE1 activity assay to determine their percent inhibition of APE1 catalytic activity relative to a protein-only control. The assay used to derive activity data for compounds is schematically shown in Figure 5A. Of the 80 compounds selected for screening, 46 compounds inhibited APE1 catalytic activity with an IC<sub>50</sub> value less than 100 μM (Figure 4B). Approximately 60% of screened compounds that were retrieved by pharmacophore models (H1NI2, A1NI2, and A3NI1) bearing at least one negatively ionizable feature showed potential inhibitory activity against APE1. Structure and APE1 inhibitory activity of the most active compounds **1–21** are given in Table 1. The moderately active compounds **S1–S25** (IC<sub>50</sub> values of >26 μM and <100 μM) and inactive compounds **S26–S59** (IC<sub>50</sub> > 100 μM) are given in Tables S1 and S2 (Supporting Information). Surprisingly, a very low number of compounds retrieved by the shape-merged pharmacophore model S1A3H1 inhibited APE1 activity. Of the 80 compounds screened, only two compounds (**S60** and **S61**) showed moderate inhibitory potency against APE1 catalytic activity (Table S3, Supporting Information). The structures of inactive compounds **S62–S139** that were retrieved by pharmacophore S1A3H1 are given in Table S4 (Supporting Information). The poor performance of the pharmacophore S1A3H1 retrieved compounds in an in vitro assay is attributed to absence of a negatively ionizable feature in the pharmacophore. The presence of a negatively ionizable feature in the moderately active compounds **S60** and **S61** (Supporting Information) supports this observation. This study demonstrates the importance of selection of pharmacophore features when pharmacophore hypotheses are generated exclusively based on the chemical nature of key interactions observed between substrate and receptor. For APE1, the negatively ionizable feature represents key interactions between the abasic DNA and the active site. As envisaged by the pharmacophore models H1NI2 and A1NI2, the most potent compounds **1, 2, 5, 10, 17–20**, possessing two negatively ionizable carboxylate



**Table 5.** APE1 Inhibitory Activity of Analogues of Compound **17**

S. No.	Structure	Activity IC <sub>50</sub> (μM)
<b>17</b> A1NI2- A3NI1	 4-((2-carboxyphenoxy)methyl)-2,5-dimethylfuran-3-carboxylic acid	6 ± 1.0
<b>31</b>	 3-((3,4-dimethylphenoxy)methyl)furan-2-carboxylic acid	5 ± 2
<b>32</b>	 3-((pyridin-2-ylthio)methyl)benzofuran-2-carboxylic acid	6 ± 1
<b>33</b>	 3-((3,4-dimethylphenoxy)methyl)furan-2-carboxylic acid	11 ± 2
<b>34</b>	 3-((pyridin-2-ylthio)methyl)benzofuran-2-carboxylic acid	27 ± 1
<b>35</b>	 5-(((tetrahydrofuran-2-yl)methylthio)methyl)-2-methylfuran-3-carboxylic acid	16 ± 5

**Table 6.** Relative Inhibition Activities of APE1 Inhibitors with Exonuclease III, Endonuclease IV, and HIV-1 Integrase

compd	APE1 catalysis (IC <sub>50</sub> , μM)	ExoIII catalysis (IC <sub>50</sub> , μM)	selectivity index for APE1 inhibitors with ExoIII	EndoIV catalysis (IC <sub>50</sub> , μM)	HIV1 IN catalysis (IC <sub>50</sub> , μM)
<b>17</b>	6 ± 1	98	16	>100	>100
<b>18</b>	6 ± 1	70	12	>100	>100
<b>1</b>	4 ± 1	>100	~25	>100	>100
<b>20</b>	4 ± 1	80	20	>100	>100
<b>10</b>	6 ± 3	60	10	>100	>100
<b>5</b>	4 ± 1	90	23	>100	>100

**Table 7.** Docking Scores of the Most Potent APE1 Inhibitors for APE1 and ExoIII

compd	inhibition of APE1 catalysis (IC <sub>50</sub> , μM)	eHITS docking score for APE1	eHITS docking score for ExoIII
<b>17</b>	6 ± 1	-2.904	-1.923
<b>18</b>	6 ± 1	-2.858	-0.465
<b>1</b>	4 ± 1	-4.734	-1.890
<b>20</b>	4 ± 1	-1.789	-3.585
<b>10</b>	6 ± 3	-3.289	-2.602
<b>5</b>	4 ± 1	-4.664	-2.601

groups, inhibited APE1 activity with an IC<sub>50</sub> value of <10 μM (Table 1). Conversely, some of the inactive compounds possessing one or two negatively ionizable groups indicate that mere presence of the negatively ionizable features alone does not confer activity to compounds (Table S2, Supporting Information). The presence and optimal arrangement of functional groups complementary to the chemical environment of the APE1 active site, including negatively ionizable features, are required for a compound to inhibit APE1 catalytic activity. In general, the structure and inhibitory profile of screened compounds demonstrate that the presence of at least one negatively ionizable feature is required for APE1 inhibition. Activity profiles of some of the potent compounds that inhibited APE1-mediated cleavage of a synthetic oligonucleotide containing an abasic site analogue (tetrahydrofuran) with IC<sub>50</sub> values below 10 μM are shown in Figure 5B (Table 1).

Compounds **1** and **2** were retrieved by pharmacophore model H1NI2 and inhibited APE1 activity with IC<sub>50</sub> values of 4 and 9, respectively. The mapping of compound **1** onto model H1NI2 shows an excellent agreement with pharmacophore fit value of 2.84 out of 3.0 between chemical features of **1** and pharmacophoric features of model H1NI2 (Figure 6A). Pharmacophore model H1NI2 demonstrated high predictive ability by retrieving (80%) active compounds (Figure 4B). Of the six compounds selected for screening from H1NI2, 5 compounds **1–2** and **S1–S3** (Supporting Information) inhibited APE1 activity with an IC<sub>50</sub> value of <100 μM (Table 1 and Table S1 of the Supporting Information). The promising APE1 inhibitory activity and high fit value of compounds **1** and **2** onto pharmacophore H1NI2 encouraged us to explore the small-molecule databases to identify readily available analogues. Two retrieved analogue compounds of **1** and **2** were screened in the APE1 assay. Compounds **22** bearing a *para* tolyl and **23** with a 4-fluoro phenyl at the 5-position of the pyrrole core inhibited APE1 activity with IC<sub>50</sub> values of 12 and 9 μM. (Table 2).

All the compounds were docked on to the active site of APE1 using GOLD. The docking was carried out to predict the possible binding conformations and interactions of the compounds inside the active site of APE1. The predicted binding conformation of compound **1** inside the active site of APE1 demonstrates excellent agreement between binding interactions and pharma-



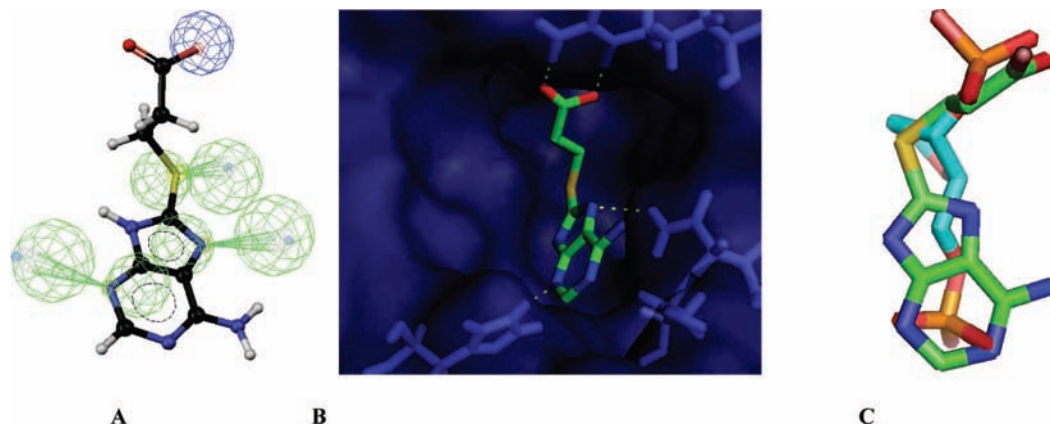


**Figure 8.** (A) Compound **21** mapped onto pharmacophore A3NI1. There is a good agreement between chemical features of compound **21** and pharmacophoric features of A3NI1. (B) The predicted bound conformation of compound **21** inside the abasic DNA binding site of APE1. The blue surface represents abasic DNA binding region of APE1. Compound **21** is shown as a green stick model. Compound **21** interactions with prominent amino acid residues (stick models) of APE1 are shown as dashed lines. There is a strong agreement between mapped pharmacophoric features of compound **21** and its interactions with prominent amino acid residues of APE1 active site. (C) The predicted bound conformation of compound **21** is superimposed onto the bound orientation of abasic unit in the cocrystal structure of APE1-abasic DNA complex (PDB: 1DEW).

cophore features of H1NI2 (Figure 6B). It also shows that the 1-methyl carboxylate on the pyrrole core of compound **1** interacts with the side chain guanidine of Arg177. This charge interaction is represented by one of the NI features in pharmacophore H1NI2. The 2-propanoate on the pyrrole core of compound **1** represents the second NI feature of pharmacophore H1NI2 and forms strong H-bonding interactions with Asn174, Asn212, and His309. The pyrrole core of compound **1** representing the hydrophobic H1 feature occupied a deep hydrophobic cavity surrounded by amino acid residues Phe253, Trp280, and Ile282. The superimposition shows a high similarity in structural and chemical features of bound conformation of compound **1** and the abasic fragment from the cocrystal structure of APE1 in complex with abasic DNA (Figure 6C). The limited structure–activity relationship information and predicted binding conformation of compound **1** indicate that further modifications on the pyrrole core to fill the deep hydrophobic cavity of the active site of APE1 could enhance activity.

Compound **3** was retrieved using pharmacophore A1NI2. Similar to H1NI2, A1NI2 also demonstrated high predictive ability and excellent hit rate (85%) in retrieving potential APE1 inhibitors (Figure 4B). Of the seven compounds retrieved by pharmacophore A1NI2, five compounds (**3**, **S4**–**S7** (Supporting Information)) inhibited APE1 activity with an  $IC_{50}$  value of  $<100\ \mu\text{M}$  (Table 1 and Table S1 of the Supporting Information). Compound **3**, a symmetric dicarboxylate with a thio-diazole central core, inhibited APE1 activity with an  $IC_{50}$  value of  $17\ \mu\text{M}$  (Table 1).

Compounds **4**–**16** are common hits for pharmacophore H1NI2 and A1NI2 (Table 1). Pharmacophore models H1NI2 and A1NI2 together demonstrated a significant predictive ability (79.4%) in retrieving active compounds compared to their individual performance (Figure 4B). Of the 30 common compounds selected for screening, 23 compounds (**4**–**16** and **S8**–**S17** (Supporting Information)) inhibited APE1 activity with an  $IC_{50}$  value of  $<100\ \mu\text{M}$ . The APE1 inhibitory profile of common hits with pharmacophore models H1NI2 and A1NI2 indicates that along with the two terminal fingerprint NI features, an optimum sized central hydrophobic core with or without a favorably substituted H-bond acceptor functional group is essential for a compound to be recognized by APE1 and inhibit its activity. Compounds **5** with three carboxylate groups on the central aryl system inhibited and a hetero aryl central core

inhibited APE1 activity with  $IC_{50}$  values of  $4\ \mu\text{M}$ . The tricarboxylate **5** and its two analogues (**24**–**25**) showed strong APE1 inhibitory activity (Tables 1 and 3). Compound **5** inhibited APE1 activity with an  $IC_{50}$  value of  $4\ \mu\text{M}$ . Compounds **24** and **25** inhibited APE1 activity with  $IC_{50}$  values of 6 and  $10\ \mu\text{M}$ , respectively.

Compounds **6**–**9** are dicarboxylates bearing a substituted central hydrophobic core (Table 1). The compounds possessed reasonably sized central hydrophobic cores substituted with H-bond acceptor groups. The interfeature distance between the two NI features varies across these compounds, for example, compounds **6** and **7**. The APE1 inhibitory activity of compound **6** and **7** indicates that these compounds have an optimum arrangement of two NI, hydrophobic and H-bond acceptor features. The furan-2-carboxylate analogues **8** and **9** inhibited APE1 activity with  $IC_{50}$  values of 22 and  $20\ \mu\text{M}$ , respectively. Compounds **8** and **9** possessed two NI features and an H-bond acceptor in the central part of the compounds. The slight reduction in potency of these compounds may be due to lack of an optimum sized hydrophobic central core. Insertion of an optimum sized hydrophobic group between two NI features of compounds **8** and **9** could further enhance APE1 inhibitory activity of the compounds.

Compounds **10** and **11**, possessing a 2-oxoindole and a thioxothiazolidinone core group flanked by two carboxylate groups, exhibited strong APE1 inhibitory activity. Several analogues (**26**–**30**) of compounds **10** and **11** also showed strong APE1 inhibitory activity (Table 4). Compound **27** is the most potent among this set of compounds and inhibited APE1 activity with an  $IC_{50}$  value of  $3\ \mu\text{M}$ . Interestingly, compounds **28**–**30** possessing only one carboxylate group exhibited APE1 inhibitory activity in a range similar to that of compounds **10** and **11**. The activity profile of compounds **28**–**30** indicates that at least one carboxylate group is required for a compound to be recognized by APE1. Compound **12** is a dicarboxylate possessing a bulky hydrophobic benzocoumarin central core, which inhibited APE1 activity at an  $IC_{50}$  value of  $8\ \mu\text{M}$ . Dicarboxylate **13** possessing a bulky benzodifuranone central core also showed strong APE1 inhibitory activity. Compound **13** inhibited APE1 activity with an  $IC_{50}$  value of  $11\ \mu\text{M}$ . Similarly, dicarboxylates **14**–**16** possessing moderate to bulky hydrophobic central cores showed moderate APE1 inhibitory activity (Table 1).

Compounds **17–20** are hits common to pharmacophore models A1NI2 and A3NI1. All four compounds selected for screening inhibited APE1 activity with an  $IC_{50}$  value of  $<25 \mu M$ . Together, pharmacophore models A1NI2 and A3NI1 showed excellent predictive ability (100%) in retrieving potential APE1 inhibitors (Figure 4B). Compound **17**, a 2,5-dimethyl-3-carboxy-4-furyl-methyl salicylic acid, inhibited APE1 activity with an  $IC_{50}$  value of  $6 \pm 1 \mu M$ . The activity profile of the compound supports the observed agreement between mapped A1NI2 pharmacophore features onto compound **17** and its predicted binding interactions inside the APE1 active site (Figure 7). Taking into consideration its binding interactions with APE1 active site and mapping pattern onto pharmacophore models A1NI2 and A3NI1, a set of additional analogues were selected and screened. Most of the tested analogues (**31–35**) inhibited APE1 with an  $IC_{50}$  value similar to the parent compound (Table 5). The inhibitory profile of compound **17** and its analogues shows an inherent SAR in this class of compounds. Compound **18**, a dicarboxylate containing a central core with hydrophobic and H-bond acceptor features, also showed strong APE1 inhibitory activity. The symmetric dicarboxylates **19** and **20** also inhibited APE1 activity with  $IC_{50}$  values of 8 and  $4 \mu M$ , respectively. It is interesting to note that several APE1 inhibitors reported here, for example, compounds **3**, **6**, **7**, **13**, **16**, **19**, and **20**, are symmetric molecules. The inhibitory profile of the symmetric compounds and the symmetric nature of pharmacophore models H1NI2 and A1NI2 reveal the architecture and chemical nature of APE1 active site.

Compound **21** was retrieved by pharmacophore A3NI1. Compared to H1NI2 and A1NI2, pharmacophore A3NI1 showed low predictability (22.5%) in retrieval of potential APE1 inhibitors. Of 31 compounds selected for screening, 7 compounds (**21**, **S8–S13** (Supporting Information)) inhibited APE1 activity with an  $IC_{50}$  value of  $<100 \mu M$  (Table 1 and Table S1 of the Supporting Information). Compound **21**, a 6-amino-9H-purin-8-ylthio-3-propanoate inhibited APE1 activity with an  $IC_{50}$  value of  $20 \mu M$ . An excellent correlation is observed between pharmacophore mapping and predicted binding interactions of compound **21** inside the active site of APE1 (Figure 7A–B). The predicted binding conformation of compound **21** demonstrates that the carboxylate (propanoate) group of the compound that is mapped by a NI feature of pharmacophore A3NI1 forms a strong charge interaction with the side chain guanidine of Arg177. Similarly, the 6-aminopurinyll core of the compound **21**, which is mapped by two H-bond acceptor features of the pharmacophore A3NI1, is involved in two H-bond acceptor interactions with amino acid residues His309 and Asn174 (Figure 7A–B). The superimposition of the predicted bound conformation of compound **21** onto the abasic DNA fragment shows a high similarity in nature and position of key chemical features of the molecules (Figure 7C). A good match between the mapping pattern of key pharmacophore features with predicted binding interactions inside the active site supports the APE1 inhibitory profile of compound **21**.

To assess the specificity toward APE1 of a sample of the most potent APE1 inhibitors, we examined their activity in three other proteins that are either functionally or structurally homologous to APE1 (ExoIII), originating from a different family of abasic endonucleases (EndoIV) or exhibiting similar DNA phosphate backbone cleavage activity (HIV-1 integrase). ExoIII and EndoIV represent two distinct protein families based on the two major abasic endonucleases found in *E. coli* but do not exhibit any similarity in either structure or catalytic mechanism to each other.<sup>4</sup> ExoIII shares significant functional

homology with APE1 and is thus a valid candidate to experimentally determine the overall specificity of these molecules toward this family of abasic endonucleases as well as preferential inhibition of human APE1 over its bacterial counterpart using our assay. As predicted, the overall trend of inhibition by these molecules is prevalent with ExoIII. However, the  $IC_{50}$  value and selectivity index of the inhibitors for the same experimental concentrations of ExoIII are markedly higher (up to 20-fold) than the relative values for APE1, suggesting a molecular selectivity for the human enzyme based on differences in key ligand-interacting amino acid residues within the active site of the respective proteins (Table 6).

In contrast to the prevalent, though not comparable, activity of our lead molecules against APE1 and ExoIII, the counter-screen performed using EndoIV and HIV-1 integrase indicates complete loss of activity. EndoIV is a major abasic endonuclease in bacteria for which a human counterpart has not been identified and operates to cleave at abasic sites in DNA via a similar hydrolytic mechanism to the ExoIII-like endonucleases. Despite showing comparable incision rates for double-stranded synthetic oligonucleotides containing a tetrahydrofuranyl residue, EndoIV displays substantial difference in substrate preference over ExoIII.<sup>38</sup> The hydrophobic pockets of ExoIII (comprising residues Trp212, Leu226, and Ile228) and APE1 (comprising Phe266, Trp280, and Leu282) contribute to substrate selectivity of the ExoIII family members, and the results of these experiments indicate selective inhibition by these compounds of the family of ExoIII-like proteins. Docking scores were generated using eHITS software for each of the selected small molecules with APE1 and ExoIII, respectively, also indicate selectivity for the human enzyme with the exception of compound **20** (Table 7).<sup>39</sup>

HIV-1 integrase is a retroviral enzyme that mediates integration of viral DNA into the host genome. Cleavage of the sugar–phosphate backbone at a dinucleotide adjacent to a conserved CA on reverse-transcribed viral DNA results in a 3'-hydroxyl moiety for subsequent enzymatic catalysis. Similar to APE1 catalysis, and indeed that of most DNA-binding enzymes, the presence of a divalent metal cation is required for efficient integration.<sup>40</sup> The most potent APE1-inhibitory compounds did not show any activity against HIV-1 integrase. Given that the predominant functional moieties of these compounds are dicarboxylate groups, the mechanism of inhibition of these molecules might be suggestive of metal chelation. Indeed, beta-diketo acids form a well-studied class of HIV-1 integrase inhibitors whose primary mode of inhibition is metal chelation.<sup>41</sup> However, because the HIV-1 integrase reaction in our assays takes place in the presence of a divalent  $Mn^{2+}$  cation and proceeds unchecked in the presence of the APE1 inhibitory molecules, it is unlikely that metal chelation reaction by free acid groups is the mode of inhibition in this case. Table 6 summarizes the relative activities of the six most potent APE1 inhibitors with ExoIII, EndoIV, and HIV-1 integrase. The selectivity index is the calculated fold-change in  $IC_{50}$  value of the APE1 inhibitors for ExoIII. In addition to the enzymes above, these molecules do not inhibit restriction endonuclease activity of EcoRI and BamHI (data not shown).

The results of these experiments to ascertain specificity of these molecules for inhibition of APE1 and other ExoIII-like endonucleases also negates the possibility that the mechanism of inhibition involved is direct binding to the abasic site itself within DNA, such as that of methoxyamine.<sup>42</sup> Because of the distinct selectivity of these molecules to prevent incision by APE1 and ExoIII, it may be argued that they target the catalytic

or DNA-binding residues within the respective active sites of these enzymes. In addition to the small molecules presented in this study as direct inhibitors to APE1 catalysis, molecules found to target APE1 allosteric sites leading to altered DNA binding, or the interruption of protein–protein interactions essential for DNA repair, may also find clinical success as potentiators of DNA-damaging agents by specific disruption of the BER pathway.

## Conclusion

In this report, we have demonstrated successful rational design of small-molecule APE1 inhibitors, using a set of 3D pharmacophore models that were generated based on key interactions of the abasic DNA within the APE1 catalytic active site. The most potent and selective inhibitors with IC<sub>50</sub> values below 10  $\mu$ M are those containing two carboxylate functional groups in a 3D arrangement with hydrophobic groups, similar to that of the arrangement of the 3'- and 5'- deoxyribosephosphate groups on abasic DNA. The APE1 inhibitory profile of some of the most potent compounds indicates that along with two terminal fingerprint negatively ionizable features or bioisostere groups of negatively ionizable features, an optimum sized central hydrophobic core with or without a favorably substituted H-bond acceptor/donor functional group is essential for a compound being recognized by APE1 and inhibit its catalytic activity. The observed resemblance between mapping of representative pharmacophore models such as H1NI2 and A1NI2 on to the most potent compounds and their predicted binding conformations (key interactions) inside APE1 active site reveals the chemical environment and architecture of the active site of APE1. The presence and optimal arrangement of functional groups complementary to the chemical environment of the APE1 active site are required for a compound to inhibit APE1 catalytic activity. Our assessment of the chemical, steric, and electrostatic nature of the APE1 active site has refined the identification of interactions between abasic DNA and residues within the active site that translate to efficient inhibition of catalysis. Furthermore, limited structure–activity analysis of all of the small molecules tested as part of this study, as well as the potent compounds themselves, will form an informative structural platform for the rational optimization of lead compounds to selective small-molecule inhibitors of APE1.

## Experimental Section

**Generation of Pharmacophore Models.** The 3D pharmacophore models were generated using the abasic DNA fragment as a template. The abasic fragment, 3',5'-deoxyribose phosphate was extracted from the cocrystal structures of human APE1 bound abasic DNA (PDBs: 1DEW and 1DE9).<sup>36</sup> The coordinates of abasic fragment were exported to Catalyst (Accelrys, Inc.) for pharmacophore mapping.<sup>43</sup> Using the Pharmacophore View/Map work bench, the abasic fragment was explored to identify presence of various pharmacophore features. A set of pharmacophore features were selected to represent key interactions observed between the abasic site and the active site of APE1 in the cocrystal structures of human APE1 bound abasic DNA. The pharmacophore features selected are negatively ionizable (NI), hydrophobic (H), and H-bond acceptor (A) features. Features were first mapped onto the abasic fragment. Reasonable features were then selected and merged into searchable 3D pharmacophore models. Four pharmacophore models H1NI2, A1NI2, A3NI1, and H1A3, were generated by combining NI, H, and A features.

**GOLD Docking Simulations.** Predicted binding interactions of compounds within the APE1 active site were generated using GOLD docking software. Compounds with free carboxyl groups were modeled in their carboxylate form as this form is considered

biologically relevant. All the water molecules present in protein were removed, and hydrogen atoms were added to the protein considering appropriate ionization states for both the acidic and basic amino acid residues. Docking was performed using version 3.2 of the genetic optimization for ligand docking (GOLD) (Cambridge Crystallographic Data Centre) software package.<sup>37,44,45</sup> A 20 Å radius active site was defined using the backbone N atom of amino acid residue A174 as the center of the active site. All the compounds were docked into the active site of the APE1. On the basis of the GOLD fitness score, for each molecule, a bound conformation with high fitness score was considered as the best bound conformation. All docking runs were carried out using standard default settings with a population size of 100, a maximum number of 100000 operations, and a mutation and crossover rate of 95. The fitness function that was implemented in GOLD consisted basically of H-bonding, complex energy, and ligand internal energy terms.

**Docking Studies using eHITS.** Docking studies were carried out using GOLD and eHITS programs. eHITS evaluates all the possible protonation states for the receptor and ligands automatically for every receptor–ligand pair and systematically covers the part of the conformational and positional search space to avoid severe steric clashes. Our docking tasks were performed on APE1 (PDB ID: 1DE9) and ExoIII (PDB ID: 1AKO). The two structures were first aligned based on their pair-wised sequence alignment. The high degree of sequence identity and homology between the two enzymes allowed us to use a highly conserved aspartic acid residue (Asp151 in ExoIII and Asp210 in APE1) as a clip file to align enzymes.

**Oligonucleotides.** For the APE1, ExoIII, and EndoIV enzymes the following oligonucleotides were used: The top strand (5'-ATTTCACCGGTACG(F)TCTAGAATCCG-3') containing the tetrahydrofuran synthetic abasic residue (F) and the bottom strand (3'-TAAAGTGCCATGC(C)AGATCTTAGGC-5'). The HIV-1 integrase catalytic assay uses 21-top (5'-GTGTGGAAAATCTCTAGCAGT-3') and 21-bot (5'-ACTGCTAGAGATTTCCACAC-3') oligonucleotides specifically recognized by the enzyme for catalysis.

**Biological Materials, Chemicals and Enzymes.** All compounds were dissolved in DMSO to a final stock concentration of 10 mM and stored at –20 °C. Dilutions were performed in DMSO. The expression system for APE1 was a kind gift from the laboratory of Dr. Tom Curran, Department of Developmental Neurobiology, St. Jude Children's Research Hospital, Memphis, TN. Wild-type integrase was purified from an expression system generously provided by Dr. Robert Craigie, Laboratory of Molecular Biology, NIDDK, NIH, Bethesda, MD. ExoIII, EndoIV, and the restriction endonucleases were purchased from New England Biosciences (Ipswich, MA). The synthetic oligonucleotide containing a tetrahydrofuran abasic site analogue was purchased from The Midland Certified Reagent Company (Midland, TX). The oligonucleotides used in the HIV-1 integrase activity assay were purchased from Integrated DNA Technologies (Coralville, Iowa).

**Preparation of Oligo Substrate.** Top strand (5'-ATTTCACCGGTACG(F)TCTAGAATCCG 3') containing the tetrahydrofuran synthetic abasic residue (F) is radiolabeled with  $\gamma$ -P<sup>32</sup> using T4 polynucleotide kinase (Epicenter, Madison WI).

The complementary strand (3'-TAAAGTGCCATGC(C)AGATCTTAGGC-5') is added in 1.5 molar excess after deactivation of the kinase by heating to 95 °C and annealed by allowing to cool slowly to room temperature. The resulting cooled mixture is centrifuged through a Spin-25 mini-column (USA Scientific, Ocala, FL) to separate annealed double-stranded oligonucleotide from unincorporated material. The oligonucleotides used in the HIV-1 activity assays, 21-top (5'-GTGTGGAAAATCTCTAGCAGT-3'), and 21-bot (5'-ACTGCTAGAGATTTCCACAC-3') were labeled using a similar protocol.

**Purification of Recombinant, His-tagged APE1.** His-tagged APE1 was purified from *Escherichia coli* M15 cells (Qiagen, Valencia, CA). Qiagen protocol was used to generate competent M15 cells. Briefly, a pellet of bacterial cells from an overnight culture was resuspended in TFB1 buffer (100 mM RbCl, 50 mM MnCl<sub>2</sub>, 30 mM potassium acetate, 10 mM CaCl<sub>2</sub>, 15% glycerol)



and incubated on ice for 90 min. The cells were then recollected by centrifugation at 4000g for 5 min at 4 °C and then resuspended in TFB2 buffer (10 mM MOPS, 10 mM RbCl, 75 mM CaCl<sub>2</sub>, 15% glycerol). An aliquot of these cells were transformed with a Qiagen pQE30 plasmid containing the APE1 gene sequence and ampicillin resistance. The APE1 plasmid was expressed in the M15 expression strain after induction by IPTG (1 mM) at an absorbance of 0.6–0.8 optical density at 595 nm. The culture was allowed to grow for an additional 3–4 h at 37 °C. This was followed by centrifugation of the cells at 3000 rpm in a bucket rotor centrifuge (Beckman) for 20 min. Pelleted cells were resuspended in lysis buffer (20 mM HEPES, pH 7.5, 5 mM imidazole, 100 mM NaCl) and passed twice through a French Press (Thermo Spectronic, Madison, WI). Lysate was centrifuged at 31000g and the pellet was solubilized in a buffer containing 20 mM HEPES, pH 7.5, 5 mM imidazole, and 10 mM CHAPS. Recombinant APE1 protein was purified using Ni-affinity chromatography with Swell-gel Nickel-chelated discs (Pierce, Rockford, IL). The protein was eluted from the column with increasing concentrations of imidazole from 40 mM to 1M. An aliquot of each concentration postelution was run on an SDS-PAGE gel and fractions containing protein were dialyzed in Spectra/Por molecular porous membrane tubing, MWCO 12–14000 (Spectrum Laboratories, Inc., Houston, TX). The protein was dialyzed in buffer containing 20 mM HEPES, pH 7.5, 500 mM NaCl, 40% glycerol, 0.2 mM EDTA, and 1 mM dithiothreitol (DTT). After dialysis, the purified enzyme solution contained 50 mM NaCl, 1 mM HEPES, pH 7.5, 50 μM EDTA, 50 μM DTT, and 10% glycerol (w/v). Aliquots of the protein were then stored at –80 °C and removed when necessary for use.

**Enzymatic Assays.** To determine the extent of abasic residue cleavage by APE1, ExoIII, and EndoIV, or integration by HIV-1 integrase, recombinant APE1 was preincubated at a final concentration of 0.05 nM with the potential inhibitors in reaction buffer (50 mM NaCl, 1 mM HEPES, pH 7.5, 50 μM EDTA, 50 μM dithiothreitol, 10% glycerol (w/v), 7.5 mM MnCl<sub>2</sub>, 0.1 mg/mL bovine serum albumin, 10 mM 2-mercaptoethanol, 10% DMSO, and 25 mM MOPS, pH 7.2) at 30 °C for 10 min. Then, 200 nM of the 5'-end <sup>32</sup>P-labeled linear oligonucleotide substrate was added, and incubation was continued for an additional 10 minutes. Reactions were quenched by the addition of an equal volume (16 μL) of loading dye (98% deionized formamide, 10 mM EDTA, 0.025% xylene cyanol, and 0.025% bromophenol blue). An aliquot (5 μL) was electrophoresed on a denaturing 20% polyacrylamide gel (0.09 M tris-borate pH 8.3, 2 mM EDTA, 20% acrylamide, 8 M urea). The gels were dried, exposed in a PhosphorImager cassette, analyzed using a Typhoon 8610 Variable Mode Imager (Amersham Biosciences), and quantitated using ImageQuant 5.2. The percent inhibition (% I) was calculated using the following equation: %I = 100 × [1 – (D – C)/(N – C)] where C, N, and D are the fractions of 26-mer substrate converted to 13-mer incision products (or integration products) for DNA alone, DNA plus enzyme, and enzyme plus drug, respectively. The IC<sub>50</sub> values were determined by plotting the logarithm of drug concentration against percent inhibition of enzymatic activity. The optimum concentration of APE1 protein in the assay is the concentration at which there is complete conversion of the synthetic abasic-site containing oligonucleotide substrate to its cleaved product without subsequent exonuclease activity. Additional assay optimization information can be found in Supporting Information and Figure S1.

**Restriction Endonuclease Assays.** Primers (BamHI sequence: GATCGGATCCTCACAGTGCTAGGT ATAGGGT; EcoRI sequence: CCGGAATTCATGCCGAAGCGTGGAAAAAGG) containing the appropriate restriction sites were incubated with the enzyme and the inhibitory molecules at 10 μM for 3 h at 37 °C. The products of these reactions were electrophoresed on a 0.5% agarose gel containing ethidium bromide and visualized under UV light using a Biorad ChemiDoc XRS system (Biorad).

**Acknowledgment.** This study was supported by funds from the Susan G. Komen Breast Cancer Foundation and Norris Cancer Center Pre-Doctoral Award at the University of Southern

California. We also thank Dr. Laith Q. Al-Mawsawi for critical reading of the manuscript and Calvin Moh for assistance with experiments.

**Supporting Information Available:** Optimization of assay conditions for screening small-molecule inhibitors to APE1 catalysis. In addition, data and structures for moderately active and inactive compounds (Tables S1–S4), and purity data (NMR) for all compounds reported in this manuscript is provided. This material is available free of charge via the Internet at <http://pubs.acs.org>.

## References

- (1) Hoeijmakers, J. H. Genome maintenance mechanisms for preventing cancer. *Nature* **2001**, *411*, 366–374.
- (2) Chen, D. S.; Herman, T.; Demple, B. Two distinct human DNA diesterases that hydrolyze 3'-blocking deoxyribose fragments from oxidized DNA. *Nucleic Acids Res.* **1991**, *19*, 5907–5914.
- (3) Hadi, M. Z.; Wilson, D. M., III. Second human protein with homology to the *Escherichia coli* abasic endonuclease exonuclease III. *Environ. Mol. Mutagen.* **2000**, *36*, 312–324.
- (4) Wilson, D. M., III.; Barsky, D. The major human abasic endonuclease: formation, consequences and repair of abasic lesions in DNA. *Mutat. Res.* **2001**, *485*, 283–307.
- (5) Ramotar, D. The apurinic–apyrimidinic endonuclease IV family of DNA repair enzymes. *Biochem. Cell Biol.* **1997**, *75*, 327–336.
- (6) Mitra, S.; Hazra, T. K.; Roy, R.; Ikeda, S.; Biswas, T.; Lock, J.; Boldogh, I.; Izumi, T. Complexities of DNA base excision repair in mammalian cells. *Mol. Cells* **1997**, *7*, 305–312.
- (7) Demple, B.; Harrison, L. Repair of oxidative damage to DNA: enzymology and biology. *Annu. Rev. Biochem.* **1994**, *63*, 915–948.
- (8) Winters, T. A.; Henner, W. D.; Russell, P. S.; McCullough, A.; Jorgensen, T. J. Removal of 3'-phosphoglycolate from DNA strand-break damage in an oligonucleotide substrate by recombinant human apurinic/apyrimidinic endonuclease 1. *Nucleic Acids Res.* **1994**, *22*, 1866–1873.
- (9) Suh, D.; Wilson, D. M., III.; Povirk, L. F. 3'-phosphodiesterase activity of human apurinic/apyrimidinic endonuclease at DNA double-strand break ends. *Nucleic Acids Res.* **1997**, *25*, 2495–2500.
- (10) Marenstein, D. R.; Wilson, D. M., III.; Teebor, G. W. Human AP endonuclease (APE1) demonstrates endonucleolytic activity against AP sites in single-stranded DNA. *DNA Repair* **2004**, *3*, 527–533.
- (11) Gorman, M. A.; Morera, S.; Rothwell, D. G.; de La Fortelle, E.; Mol, C. D.; Tainer, J. A.; Hickson, I. D.; Freemont, P. S. The crystal structure of the human DNA repair endonuclease HAP1 suggests the recognition of extra-helical deoxyribose at DNA abasic sites. *EMBO J.* **1997**, *16*, 6548–6558.
- (12) Dlakic, M. Functionally unrelated signalling proteins contain a fold similar to Mg<sup>2+</sup>-dependent endonucleases. *Trends Biochem. Sci.* **2000**, *25*, 272–273.
- (13) Xanthoudakis, S.; Miao, G.; Wang, F.; Pan, Y. C.; Curran, T. Redox activation of Fos-Jun DNA binding activity is mediated by a DNA repair enzyme. *EMBO J.* **1992**, *11*, 3323–3335.
- (14) Xanthoudakis, S.; Miao, G. G.; Curran, T. The redox and DNA-repair activities of Ref-1 are encoded by nonoverlapping domains. *Proc. Natl. Acad. Sci. U.S.A.* **1994**, *91*, 23–27.
- (15) Abate, C.; Patel, L.; Rauscher, F. J., III.; Curran, T. Redox regulation of fos and jun DNA-binding activity in vitro. *Science* **1990**, *249*, 1157–1161.
- (16) Silber, J. R.; Bobola, M. S.; Blank, A.; Schoeler, K. D.; Haroldson, P. D.; Huynh, M. B.; Kolstoe, D. D. The apurinic/apyrimidinic endonuclease activity of Ape1/Ref-1 contributes to human glioma cell resistance to alkylating agents and is elevated by oxidative stress. *Clin. Cancer Res.* **2002**, *8*, 3008–3018.
- (17) Chen, D. S.; Olkowski, Z. L. Biological responses of human apurinic endonuclease to radiation-induced DNA damage. *Ann. N.Y. Acad. Sci.* **1994**, *726*, 306–308.
- (18) Walker, L. J.; Craig, R. B.; Harris, A. L.; Hickson, I. D. A role for the human DNA repair enzyme HAP1 in cellular protection against DNA damaging agents and hypoxic stress. *Nucleic Acids Res.* **1994**, *22*, 4884–4889.
- (19) Fung, H.; Demple, B. A vital role for Ape1/Ref1 protein in repairing spontaneous DNA damage in human cells. *Mol. Cell* **2005**, *17*, 463–470.
- (20) McNeill, D. R.; Wilson, D. M., III. A dominant-negative form of the major human abasic endonuclease enhances cellular sensitivity to laboratory and clinical DNA-damaging agents. *Mol. Cancer Res.* **2007**, *5*, 61–70.
- (21) Puglisi, F.; Aprile, G.; Minisini, A. M.; Barbone, F.; Cataldi, P.; Tell, G.; Kelley, M. R.; Damante, G.; Beltrami, C. A.; Di Loreto, C. Prognostic significance of Ape1/ref-1 subcellular localization in non-small cell lung carcinomas. *Anticancer Res.* **2001**, *21*, 4041–4049.



- (22) Kakolyris, S.; Giatromanolaki, A.; Koukourakis, M.; Kaklamanis, L.; Kanavaros, P.; Hickson, I. D.; Barzilay, G.; Georgoulas, V.; Gatter, K. C.; Harris, A. L. Nuclear localization of human AP endonuclease 1 (HAP1/Ref-1) associates with prognosis in early operable non-small cell lung cancer (NSCLC). *J. Pathol.* **1999**, *189*, 351–357.
- (23) Kakolyris, S.; Kaklamanis, L.; Engels, K.; Fox, S. B.; Taylor, M.; Hickson, I. D.; Gatter, K. C.; Harris, A. L. Human AP endonuclease 1 (HAP1) protein expression in breast cancer correlates with lymph node status and angiogenesis. *Br. J. Cancer* **1998**, *77*, 1169–1173.
- (24) Kakolyris, S.; Kaklamanis, L.; Engels, K.; Turley, H.; Hickson, I. D.; Gatter, K. C.; Harris, A. L. Human apurinic endonuclease 1 expression in a colorectal adenoma-carcinoma sequence. *Cancer Res.* **1997**, *57*, 1794–1797.
- (25) Xu, Y.; Moore, D. H.; Broshears, J.; Liu, L.; Wilson, T. M.; Kelley, M. R. The apurinic/apyrimidinic endonuclease (APE/ref-1) DNA repair enzyme is elevated in premalignant and malignant cervical cancer. *Anticancer Res.* **1997**, *17*, 3713–3719.
- (26) Moore, D. H.; Michael, H.; Tritt, R.; Parsons, S. H.; Kelley, M. R. Alterations in the expression of the DNA repair/redox enzyme APE/ref-1 in epithelial ovarian cancers. *Clin. Cancer Res.* **2000**, *6*, 602–609.
- (27) Evans, A. R.; Limp-Foster, M.; Kelley, M. R. Going APE over ref-1. *Mutat. Res.* **2000**, *461*, 83–108.
- (28) Herring, C. J.; West, C. M.; Wilks, D. P.; Davidson, S. E.; Hunter, R. D.; Berry, P.; Forster, G.; MacKinnon, J.; Rafferty, J. A.; Elder, R. H.; Hendry, J. H.; Margison, G. P. Levels of the DNA repair enzyme human apurinic/apyrimidinic endonuclease (APE1, APEX, Ref-1) are associated with the intrinsic radiosensitivity of cervical cancers. *Br. J. Cancer* **1998**, *78*, 1128–1133.
- (29) Koukourakis, M. I.; Giatromanolaki, A.; Kakolyris, S.; Sivridis, E.; Georgoulas, V.; Funtzilas, G.; Hickson, I. D.; Gatter, K. C.; Harris, A. L. Nuclear expression of human apurinic/apyrimidinic endonuclease (HAP1/Ref-1) in head-and-neck cancer is associated with resistance to chemoradiotherapy and poor outcome. *Int. J. Radiat. Oncol. Biol. Phys.* **2001**, *50*, 27–36.
- (30) Belzile, J. P.; Choudhury, S. A.; Cournoyer, D.; Chow, T. Y. Targeting DNA repair proteins: a promising avenue for cancer gene therapy. *Curr. Gene Ther.* **2006**, *6*, 111–123.
- (31) Madhusudan, S.; Smart, F.; Shrimpton, P.; Parsons, J. L.; Gardiner, L.; Houlbrook, S.; Talbot, D. C.; Hammonds, T.; Freemont, P. A.; Sternberg, M. J.; Dianov, G. L.; Hickson, I. D. Isolation of a small molecule inhibitor of DNA base excision repair. *Nucleic Acids Res.* **2005**, *33*, 4711–4724.
- (32) Seiple, L. A.; Cardellina, J. H., II.; Akee, R.; Stivers, J. T. Potent inhibition of human apurinic/apyrimidinic endonuclease 1 by arylstibonic acids. *Mol. Pharmacol.* **2008**, *73*, 669–677.
- (33) Woon, E. C.; Threadgill, M. D. Poly(ADP-ribose)polymerase inhibition—where now? *Curr. Med. Chem.* **2005**, *12*, 2373–2392.
- (34) Griffin, R. J.; Fontana, G.; Golding, B. T.; Guiard, S.; Hardcastle, I. R.; Leahy, J. J.; Martin, N.; Richardson, C.; Rigoreau, L.; Stockley, M.; Smith, G. C. Selective benzopyranone and pyrimido[2,1-*a*]isoquinolin-4-one inhibitors of DNA-dependent protein kinase: synthesis, structure–activity studies, and radiosensitization of a human tumor cell line in vitro. *J. Med. Chem.* **2005**, *48*, 569–585.
- (35) Hardcastle, I. R.; Cockcroft, X.; Curtin, N. J.; El-Murr, M. D.; Leahy, J. J.; Stockley, M.; Golding, B. T.; Rigoreau, L.; Richardson, C.; Smith, G. C.; Griffin, R. J. Discovery of potent chromen-4-one inhibitors of the DNA-dependent protein kinase (DNA-PK) using a small-molecule library approach. *J. Med. Chem.* **2005**, *48*, 7829–7846.
- (36) Mol, C. D.; Izumi, T.; Mitra, S.; Tainer, J. A. DNA-bound structures and mutants reveal abasic DNA binding by APE1 and DNA repair coordination [corrected]. *Nature* **2000**, *403*, 451–456.
- (37) *GOLD 3.2*; The Cambridge Crystallographic Data Centre: Cambridge, UK, 2005.
- (38) Demple, B.; Harrison, L.; Wilson, D. M., 3rd.; Bennett, R. A.; Takagi, T.; Ascione, A. G. Regulation of eukaryotic abasic endonucleases and their role in genetic stability. *Environ. Health Perspect.* **1997**, *105* (Suppl 4), 931–934.
- (39) Zsoldos, Z.; Reid, D.; Simon, A.; Sadjad, B. S.; Johnson, A. P. eHiTS: an innovative approach to the docking and scoring function problems. *Curr. Protein Pept Sci.* **2006**, *7*, 421–435.
- (40) Asante-Appiah, E.; Skalka, A. M. HIV-1 integrase: structural organization, conformational changes, and catalysis. *Adv. Virus Res.* **1999**, *52*, 351–369.
- (41) Dayam, R.; Deng, J.; Neamati, N. HIV-1 integrase inhibitors: 2003–2004 update. *Med. Res. Rev.* **2006**, *26*, 271–309.
- (42) Liu, L.; Gerson, S. L. Therapeutic impact of methoxyamine: blocking repair of abasic sites in the base excision repair pathway. *Curr. Opin. Invest. Drugs* **2004**, *5*, 623–627.
- (43) *Catalyst*; Accelrys, Inc.: San Diego, CA.
- (44) Verdonk, M. L.; Chessari, G.; Cole, J. C.; Hartshorn, M. J.; Murray, C. W.; Nissink, J. W.; Taylor, R. D.; Taylor, R. Modeling water molecules in protein–ligand docking using GOLD. *J. Med. Chem.* **2005**, *48*, 6504–6515.
- (45) Verdonk, M. L.; Cole, J. C.; Hartshorn, M. J.; Murray, C. W.; Taylor, R. D. Improved protein–ligand docking using GOLD. *Proteins* **2003**, *52*, 609–623.

JM800739M